

Element-wise Multiplication Based Physics-informed Neural Networks

Feilong Jiang^a Xiaonan Hou^{a*} Min Xia^{b*}

^a Department of Engineering, Lancaster University, LA1 4YW Lancaster, U.K.

^b Department of Mechanical and Materials Engineering, University of Western Ontario, London, Ontario, Canada

x.hou2@lancaster.ac.uk

mxia47@uwo.ca

Abstract

As a promising framework for resolving partial differential equations (PDEs), physics-informed neural networks (PINNs) have received widespread attention from industrial and scientific fields. However, lack of expressive ability and initialization pathology issues are found to prevent the application of PINNs in complex PDEs. In this work, we propose Element-wise Multiplication Based Physics-informed Neural Networks (EM-PINNs) to resolve these issues. The element-wise multiplication operation is adopted to transform features into high-dimensional, non-linear spaces, which effectively enhance the expressive capability of PINNs. Benefiting from element-wise multiplication operation, EM-PINNs can eliminate the initialization pathologies of PINNs. The proposed structure is verified on various benchmarks. The results show that EM-PINNs have strong expressive ability.

1. Introduction

As an important role in scientific machine learning field, physics-informed neural networks (PINNs) appear to be a promising method for resolving partial differential equations (PDEs) [1]. Utilizing the physical laws as the constraints of neural networks, PINNs show better interpretability and generalization ability than traditional data-driven machine learning models. As an alternative of traditional numerical algorithms, PINNs have been widely applied in scientific and engineering fields [2-5].

Although promising outcomes have been presented, PINNs have been observed of failing resolving some PDEs, especially when the solutions exhibit high-frequency or multi-scale characteristics [6], [7]. Many efforts have been made to improve the capability of PINNs. To resolve the loss terms unbalancing problem, methods such as NTK-based weighting [6], Grad Norm [8] and SoftAdapt [9] are used to weight different loss term for training PINNs effectively. Utilizing the geometry-aware approximations [10] or Fourier feature embedding [11] methods, the boundary conditions can be exactly imposed during the training process. Consequently, the accuracy of PINNs can be effectively improved. Since the training process of PINNs may go against physical casualty, training methods that follow the spatio-temporal causal are proposed to improve the accuracy of PINNs [12-14]. The loss imbalance problem between different training points prevents PINNs from resolving PDEs correctly. This issue can be resolve by introducing adaptive weighting scheme [15-18] or adaptive resampling method [19], [20]. New neural network structures such as mMLP [8], Fourier feature embedding [7], DM-PINNs [21] and SPINN [22] are also proven to be useful for improving the representative capability of PINNs.

Despite the success of these research, most existing works still use small neural networks with small number of hidden layers (typically less than 9). This is attributed to the gradient vanishing issue of deep PINNs structure, which limits the representative capability of PINNs. Recent research has proofed that the gradient vanishing of PINNs is mainly related to the initialization pathologies [23]. To overcome this limitation, we propose a novel architecture

which is EM-PINNs. By doing element-wise multiplication between 2 sub-layers, the outputs of the 2 layers are fused together and projected into nonlinear-high-dimensional feature spaces. In this way the expressive ability of PINNs can be effectively improved, and initialization pathologies can be eliminated. Besides, with the stacking of a series of shortcut connected multiplication blocks, the model can use deeper neural network structure and obtain better results.

The main contributions of this paper are as follows:

- We leverage the element-wise multiplication operation to effectively improve the prediction accuracy of PINNs with relatively small increment on computing resource.
- We designed a skip connected multiplication physics-informed neural network structure to resolve the gradient vanishing problem of PINNs.
- We demonstrate the effect of EM-PINNs by conducting experiments on several benchmarks and present state-of-the-art results.

2. Related works

Physics-informed Neural Networks (PINNs)

Following the original work of physics-informed neural networks (PINNs) as outlined in [1], the typical form of partial differential equation (PDEs) can be represented as:

$$u_t + \mathcal{N}[u] = 0, \quad t \in [0, T], \quad x \in \Omega, \quad (1)$$

where u indicates the latent solution, $\mathcal{N}[\cdot]$ represents a linear or nonlinear differential operator. The initial and boundary conditions are in the forms of:

$$u(0, x) = g(x), \quad x \in \Omega, \quad (2)$$

$$\mathcal{B}[u] = 0, \quad t \in [0, T], \quad x \in \partial\Omega, \quad (3)$$

where $g(x)$ is a given function, $\mathcal{B}[\cdot]$ indicates boundary operator.

The core idea of PINNs is approximating the latent solution $u(t, x)$ with a neural network $u_\theta(t, x)$, where θ represents trainable parameters of the neural network (NN). Instead of utilizing the difference between label data $u(t, x)$ and the prediction of NN $u_\theta(t, x)$, PINNs directly utilizes the PDE and the corresponding initial and boundary conditions as the loss function. Utilizing automatic differentiation [24], the required gradients with respect to input variables can be obtained. The loss function can be expressed as:

$$\mathcal{L}(\theta) = \lambda_{ic} \mathcal{L}_{ic}(\theta) + \lambda_{bc} \mathcal{L}_{bc}(\theta) + \lambda_r \mathcal{L}_r(\theta), \quad (4)$$

where

$$\mathcal{L}_{ic}(\theta) = \frac{1}{N_{ic}} \sum_{i=1}^{N_{ic}} \left| u_\theta(0, x_{ic}^i) - g(x_{ic}^i) \right|^2, \quad (5)$$

$$\mathcal{L}_{bc}(\theta) = \frac{1}{N_{bc}} \sum_{i=1}^{N_{bc}} \left| \mathcal{B}[u_\theta](t_{bc}^i, x_{bc}^i) \right|^2, \quad (6)$$

$$\mathcal{L}_r(\theta) = \frac{1}{N_r} \sum_{i=1}^{N_r} \left| \frac{\partial u_\theta}{\partial t}(x_r^i, t_r^i) + \mathcal{N}[u_\theta](x_r^i, t_r^i) \right|^2, \quad (7)$$

λ represents the weighting coefficient, which is used to balance different loss terms [25].

Under these conditions, the training procedure of PINNs can be interpreted as solving the given PDEs without any labelled data.

Element-wise Multiplication in PINNs

Works in recent years showed that the expressive ability of PINNs could be effectively improved by incorporating the element-wise multiplication. Wang et al. proposed a modified multi-layer perceptron (mMLP) structure [8]. With two extra dense layers as encoders, element-wise multiplications are conducted with the output of each hidden layer and the 2 encoders separately. However, for this method, 2 times of element-wise multiplication operation are need for one hidden layer, which means it is more computationally expensive than our method with the same number of parameters. To enhance the expressive ability of PINNs densely multiplied PINNs (DM-PINNs) is proposed by Jiang et al. [21]. Without introducing extra trainable parameters into the neural network, the element-wise multiplication is conducted between each outputs hidden layers. Although effectively improved the accuracy of PINNs, it still suffers from the gradients vanishing problems when deep neural network is adopted. Cho et al. present the separable PINN (SPINN) [22]. In this structure, coordinates from different dimensions are input into different sub-networks. The final output is obtained by element-wise multiplying outputs of all the sub-networks. SPINN’s main task is to solve multi-dimensional PDEs, the element-wise multiplication operation is used to merge the outputs of different sub-networks, and the structure of sub-network is still MLP. That means the gradient vanishing problem of deep MLP is neglected.

3. EM-PINNs

The structure of the proposed EM-PINNs is shown in Fig.1. The inputs \mathbf{x} are fed into two fully connected layers with the same width. The outputs of the 2 layers are then element-wise multiplied to get a non-linear high-dimensional feature $\mathbf{H}^{(1)}$:

$$\mathbf{H}^{(1)} = \sigma(\mathbf{W}_1 \cdot \mathbf{x} + \mathbf{b}_1) \odot \sigma(\mathbf{W}_2 \cdot \mathbf{x} + \mathbf{b}_2), \quad (8)$$

where σ denotes activation function, \mathbf{W} represents weights, \mathbf{b} represents biases. $\mathbf{H}^{(1)}$ is then input into N shortcut connection blocks. Each shortcut connection block contains 2 element-wise multiplication layers. With $\mathbf{H}^{(l)}$ as the input of l -th block ($1 \leq l \leq N$), the forward process of each shortcut connection block can be expressed as:

$$\mathbf{h}_1^{(l)} = \sigma(\mathbf{W}_1^{(l)} \cdot \mathbf{H}^{(l)} + \mathbf{b}_1^{(l)}) \odot \sigma(\mathbf{W}_2^{(l)} \cdot \mathbf{H}^{(l)} + \mathbf{b}_2^{(l)}), \quad (9)$$

$$\mathbf{h}_2^{(l)} = \sigma(\mathbf{W}_3^{(l)} \cdot \mathbf{h}_1^{(l)} + \mathbf{b}_3^{(l)}) \odot \sigma(\mathbf{W}_4^{(l)} \cdot \mathbf{h}_1^{(l)} + \mathbf{b}_4^{(l)}), \quad (10)$$

$$\mathbf{H}^{(l+1)} = \mathbf{h}_2^{(l)} + \mathbf{H}^{(l)}, \quad (11)$$

the final output u_θ is given by:

$$u_\theta = \mathbf{H}^{(N)} \cdot \mathbf{W}^{(N+1)} + \mathbf{b}^{(N+1)}. \quad (12)$$

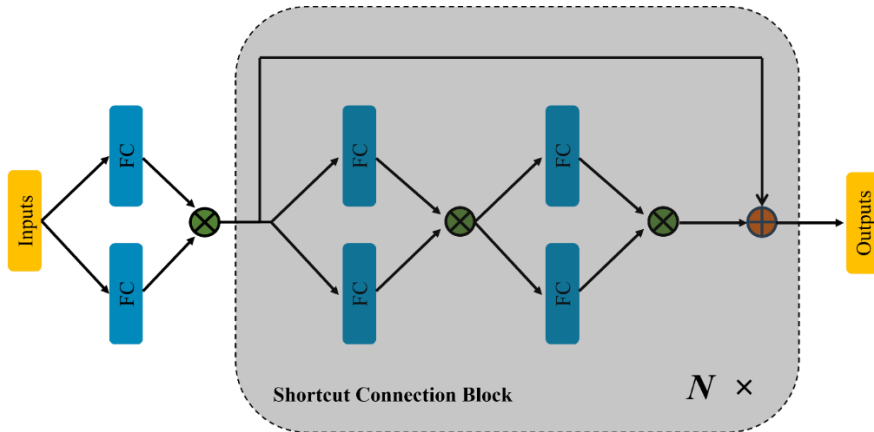


Figure 1: the structure of Deeper-PINNs.

In [23], Wang et al. verified the traditional MLP can suffer from the initialization pathology, which makes $\frac{\partial u_\theta}{\partial x}$ perform as a linear network. Under such circumstance, the model will be

hard to approximate the solution derivatives. For our method, however, the element-wise multiplication can still project the features from different subnet into a nonlinear space, which prevent the initialization pathology. The proof is shown below:

Consider the EM-PINNs without shortcut connections. With the input as x , the output $u_\theta(x)$ can be expressed as follows:

$$u_\theta^l(x) = g_1^l \odot g_2^l, g_i^l = \sigma(\mathbf{W}_i^l u_\theta^{l-1}(x) + \mathbf{b}_i^l), l=1,2,\dots,L, i=1,2, \quad (13)$$

L represents the number of hidden layers, $u_\theta^0(x) = x$. Assuming that the neural network operates within a linear regime. Under such circumstance, $\sigma(x) \approx x$. When all bias are initialized as 0, the output of the final layer is:

$$u_\theta^L(x) \approx \prod_{i=1}^L \mathbf{W}_1^i \cdot \mathbf{W}_2^{L-i+1} \cdot \mathbf{W}^{L+1} \cdot x^{2^L}. \quad (14)$$

The first-order derivate of $u_\theta(x)$ will be:

$$\frac{\partial u_\theta}{\partial x}(x) \approx 2^L \cdot \prod_{i=1}^L \mathbf{W}_1^i \cdot \mathbf{W}_2^{L-i+1} \cdot \mathbf{W}^{L+1} \cdot x^{2^L-1}. \quad (15)$$

For MLP, as give in [23], the first-order derivate of $u_\theta(x)$ under such assumption is:

$$\frac{\partial u_\theta}{\partial x}(x) \approx \mathbf{W}^{L+1} \cdot \mathbf{W}^L \cdot \dots \cdot \mathbf{W}^1. \quad (16)$$

Apparently, the MLP degrades as a deep linear network at initialization when calculating $\frac{\partial u_\theta}{\partial x}$. However, owing to the element-wise multiplication, our method still has nonlinear expressive ability.

4. Experiments

Additional enhancements

Fourier feature mapping

The Fourier feature mapping method is shown to be an effective method to improve the neural networks' expressive capability [6], [26]. The Fourier feature mapping γ can project the inputs into higher dimensional hypersphere with sine function and cosine function:

$$\gamma(\mathbf{x}) = \begin{bmatrix} \cos(\mathbf{B}\mathbf{x}) \\ \sin(\mathbf{B}\mathbf{x}) \end{bmatrix}, \quad (17)$$

each \mathbf{B} is sampled from Gaussian distribution $\mathcal{N}(0, s^2)$ with the Fourier feature scale $s > 0$.

Exact imposition of boundary conditions

By exactly imposing the boundary conditions, the loss terms corresponding to the boundary conditions can be neglected, and the training process of PINNs becomes easier. Thus, better performance can be achieved.

The Dirichlet boundary conditions can be easily imposed by approximation distance function (ADF) [10]. For such method, the output $u(\mathbf{x})$ is modified as:

$$u^{bc}(\mathbf{x}) = \phi(\mathbf{x})u(\mathbf{x}) + g(\mathbf{x}), \quad (18)$$

where $\phi(\mathbf{x})$ is a distance function that equals to 0 at the given boundaries, $g(\mathbf{x})$ represents the solution on the boundaries.

The periodic boundary conditions can be enforced by a special Fourier feature embedding [11], [27], which is given by:

$$v(x) = (1, \cos(\omega_x x), \sin(\omega_x x), \cos(2\omega_x x), \sin(2\omega_x x), \dots, \cos(m\omega_x x), \sin(m\omega_x x)), \quad (19)$$

where $\omega_x = \frac{2\pi}{P_x}$, P_x is the period in the x direction, m is a non-negative integer. The time coordinate can be directly concatenated with $v(x)$ or $v(x, y)$. For higher dimensional problem, more details can be found in [12].

Experimental setups

For all the cases, the weights are initialized with Xavier normal distribution [28], and tanh is used as the activation function. The training is conducted on a single NVIDIA GeForce RTX 4090 GPU. All the results are averaged from 5 independent trials.

Results

Allen-Cahn equation

Allen-Cahn equation is a widely used benchmark for PINNs. The equation is expressed as below:

$$u_t - 0.0001u_{xx} + 5u^3 - 5u = 0, \quad x \in [-1, 1], \quad t \in [0, 1], \quad (20)$$

$$u = 0, \quad x = x^2 \cos \pi x, \quad (21)$$

$$u(t, -1) = u(t, 1), \quad (22)$$

$$u_x(t, -1) = u_x(t, 1). \quad (23)$$

The periodic boundary condition is imposed by one-dimensional Fourier feature embedding. The embedded input can be expressed as:

$$v(x, t) = (t, 1, \cos(\omega_x x), \sin(\omega_x x), \dots, \cos(m\omega_x x), \sin(m\omega_x x)). \quad (24)$$

λ_{ic} is set as 100. The model is trained by Adam optimizer. More hyper-parameters can be found in Table 1.

Table 1: Allen-Cahn equation: Hyper-parameter configuration.

| Parameter | Value |
|----------------------------------|---------|
| Architecture Parameters | |
| Number of blocks | 4 |
| Layer size | 185 |
| Fourier feature embedding | |
| m | 10 |
| P_x | 2 |
| Training Parameters | |
| Initial learning rate | 0.001 |
| Exponential decay steps | 8,000 |
| Decay rate | 0.9 |
| Training steps | 300,000 |
| Collocation points | 25,600 |

The results of different models are shown in Table 2. It indicates that our method achieves the best result ever reported in the PINNs literature for this example. The best result of our 5 trials is presented in Fig 2. It shows good alignment with the exact solution. The relative L^2

error is $1.68\text{e-}5$, which is smaller than state-of-the-art result of this case ($2.24\text{e-}5$ [23]) with less trainable parameters.

Table2: Allen-Cahn equation: Relative L^2 error comparison between different models

| Method | Relative L^2 error |
|----------------------|-------------------------------------|
| SA weights [16] | $1.11\text{e-}4$ |
| DASA-PINNs [29] | $8.57\text{e-}5$ |
| Causal training [12] | $1.39\text{e-}4$ |
| JAX-PI [27] | $5.37\text{e-}5$ |
| RBA-PINNs [15] | $5.8\text{e-}5$ |
| Deeper-PINNs | $2.47\text{e-}05$ |

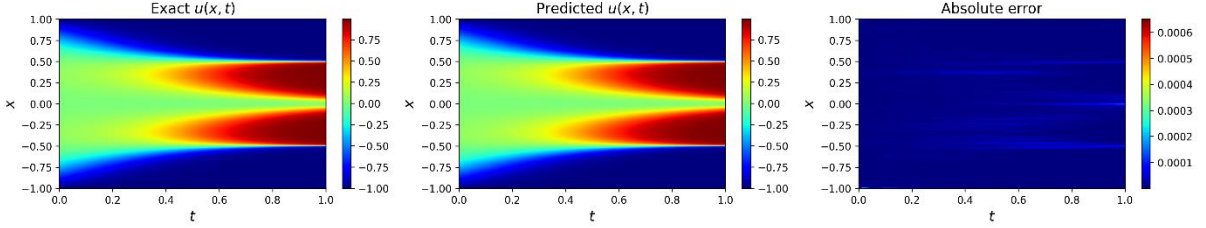


Figure 2: Allen-Cahn equation: Comparison between the prediction and the reference solution.

Helmholtz equation

We consider the 2D Helmholtz equation in the form of:

$$\frac{\partial^2 u}{\partial x^2} + \frac{\partial^2 u}{\partial y^2} + k^2 u - q(x, y) = 0, \quad x \in [-1, 1], y \in [-1, 1], \quad (25)$$

$$u(-1, y) = u(1, y) = u(x, -1) = u(x, 1) = 0, \quad (26)$$

where the source term $q(x, y)$ is in the form of:

$$\begin{aligned} q(x, y) = & -a_1 \pi^2 \sin(a_1 \pi x) \sin(a_2 \pi y) \\ & - a_2 \pi^2 \sin(a_1 \pi x) \sin(a_2 \pi y) \\ & + k^2 \sin(a_1 \pi x) \sin(a_2 \pi y) w, \end{aligned} \quad (27)$$

here we set $a_1 = 1, a_2 = 4$ and $k = 1$. The boundary conditions are directly imposed by the ADF: $(1-x^2)(1-y^2)$, thus the output $u^{bc}(x, y) = u(x, y) * (1-x^2) * (1-y^2)$. The model is trained by Adam optimizer for 500 iterations, then followed by L-BFGS for maximum 3000 iterations. Table 3 shows the details of the hyper-parameters in detail.

Table 3: Helmholtz equation: Hyper-parameter configuration.

| Parameter | Value |
|----------------------------------|--------|
| Architecture Parameters | |
| Number of blocks | 1 |
| Layer size | 64 |
| Fourier feature scale (s) | 2.0 |
| Training Parameters | |
| Learning rate of Adam | 0.005 |
| Training steps of Adam | 500 |
| Learning rate of L-BFGS | 1 |
| Maximum training steps of L-BFGS | 500 |
| Collocation points | 10,201 |

Table 4 shows the performance of the proposed method together with various existing PINNs

model on this problem. It can be observed that our method obtains the highest accuracy. The best result is shown in Fig 3. The predicted outcome shows high consistency with the exact solution, with a relative L^2 error of $2.38\text{e-}6$, which is the state-of-the-art result.

Table 4: Helmholtz equation: Relative L^2 error comparison between different models

| Method | Relative L^2 error |
|----------------------------|------------------------------------|
| SA weights [16] | $3.2\text{e-}3$ |
| DASA-PINNs [29] | $5.35\text{e-}5$ |
| Learning rate annealing[8] | $1.29\text{e-}3$ |
| RBA weights [15] | $8.21\text{e-}6$ |
| Deeper-PINNs | $3.26\text{e-}6$ |

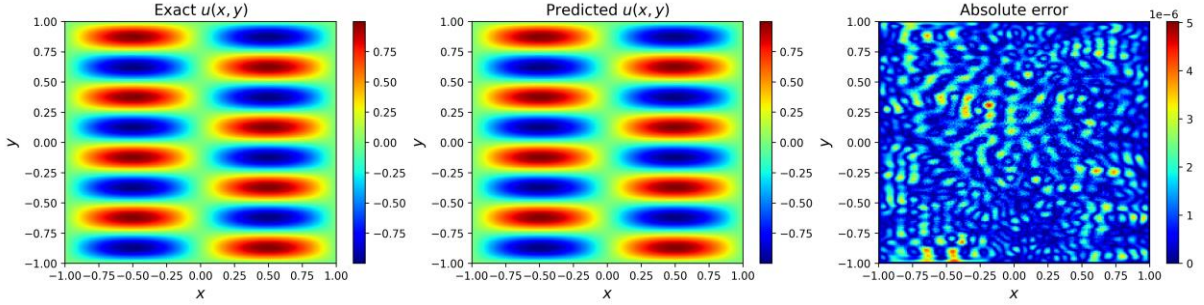


Figure 3: Helmholtz equation: Comparison of the prediction against the reference solution. The ablation study is conducted with the random seed corresponding to the best result. The outcome of ablation study is presented in Table 5. It shows that both Fourier feature mapping and ADF can effectively improve the accuracy, among which, Fourier feature mapping shows more positive influence on the result.

Table 5: Ablation study of Helmholtz equation

| Ablation Settings | | Relative L^2 error |
|-------------------|-----|------------------------------------|
| Fourier feature | ADF | |
| ✓ | ✓ | $2.38\text{e-}6$ |
| ✓ | ✗ | $3.01\text{e-}6$ |
| ✗ | ✓ | $7.27\text{e-}5$ |
| ✗ | ✗ | $3.63\text{e-}4$ |

Advection equation

To empirically demonstrate the effectiveness of our method, we consider the 1D advection equation which can be expressed as:

$$\frac{\partial u}{\partial t} + \beta \frac{\partial u}{\partial x} = 0, \quad x \in 0, 2\pi, \quad t \in 0, 1, \quad (28)$$

$$u(0, x) = \sin(x), \quad (29)$$

$$u(t, 0) = u(t, 2\pi), \quad (30)$$

Previous studies have proved that it's hard for PINNs to resolve advection equation when the transport velocity β is large. Here we set β as 100, which is a challenging task for PINNs. The periodic boundary condition is directly imposed by a special Fourier feature embedding:

$$v(x, t) = (\cos(\omega_t t), \sin(\omega_t t), 1, \cos(\omega_x x), \sin(\omega_x x)), \quad (31)$$

where $\omega_t = \frac{2\pi}{P_t}$. To prevent incorrect periodic feature, we set $P_t = 2\pi$, which is larger than

the length of the temporal domain. Thus, the embedding of t is used for improving the expressive capability of the model. More details of the hyper-parameter configuration can be

found in Table 6. The averaged relative L^2 error is $3.37\text{e-}3$. The best result is shown in Fig. 4. It shows that the prediction shows good agreement with the exact solution.

Table 6: Advection equation: Hyper-parameter configuration.

| Parameter | Value |
|--------------------------------|---------|
| Architecture Parameters | |
| Number of blocks | 22 |
| Layer size | 128 |
| Fourier feature mapping | |
| P_x | 2π |
| P_t | 2π |
| Training Parameters | |
| Initial learning rate | 0.001 |
| Exponential decay steps | 2,000 |
| Decay rate | 0.9 |
| Training steps | 100,000 |
| Collocation points | 20,000 |

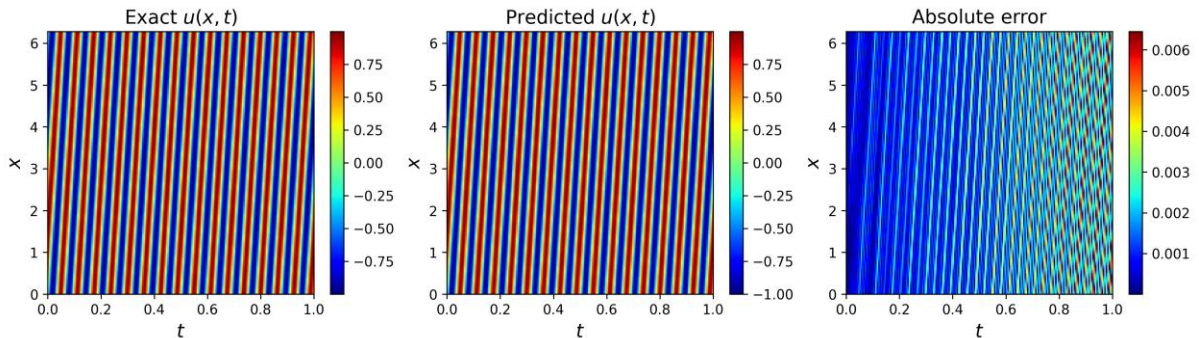


Figure 4: Advection equation: Comparison of the prediction against the exact solution. Ablation study is conducted to verify the effectiveness of different components. The results are presented in Table 7. It can be observed that by imposing the periodic boundary condition by Fourier feature embedding can significantly improve the accuracy of the model.

Table 7: Ablation study of Advection equation

| Ablation Settings | | Relative L^2 error |
|---------------------------|----------------|----------------------|
| Fourier feature embedding | Time embedding | |
| ✓ | ✓ | 3.08e-3 |
| ✓ | ✗ | 3.23e-3 |
| ✗ | ✗ | 9.80e-1 |

Conclusion

In this work, we proposed EM-PINNs, an element-wise multiplication based PINN structure. The element-wise multiplication operation could prevent the initialization pathology of PINN and at the same time improving the expressive ability of the neural network. Verifications were conducted on several benchmarks and Sota results were presented.

References

- [1] M. Raissi, P. Perdikaris, and G. E. Karniadakis, "Physics-informed neural networks: A deep learning framework for solving forward and inverse problems involving nonlinear partial differential equations," *Journal of Computational physics*, vol. 378, pp. 686-707, 2019.

- [2] S. Cai, Z. Mao, Z. Wang, M. Yin, and G. E. Karniadakis, "Physics-informed neural networks (PINNs) for fluid mechanics: A review," *Acta Mechanica Sinica*, vol. 37, no. 12, pp. 1727-1738, 2021.
- [3] S. Cai, Z. Wang, S. Wang, P. Perdikaris, and G. E. Karniadakis, "Physics-informed neural networks for heat transfer problems," *Journal of Heat Transfer*, vol. 143, no. 6, p. 060801, 2021.
- [4] F. Jiang, M. Xia, and Y. Hu, "Physics-Informed Machine Learning for Accurate Prediction of Temperature and Melt Pool Dimension in Metal Additive Manufacturing," *3D Printing and Additive Manufacturing*, 2023.
- [5] G. S. Misyris, A. Venzke, and S. Chatzivasileiadis, "Physics-informed neural networks for power systems," in *2020 IEEE power & energy society general meeting (PESGM)*, 2020: IEEE, pp. 1-5.
- [6] S. Wang, X. Yu, and P. Perdikaris, "When and why PINNs fail to train: A neural tangent kernel perspective," *Journal of Computational Physics*, vol. 449, p. 110768, 2022.
- [7] S. Wang, H. Wang, and P. Perdikaris, "On the eigenvector bias of Fourier feature networks: From regression to solving multi-scale PDEs with physics-informed neural networks," *Computer Methods in Applied Mechanics and Engineering*, vol. 384, p. 113938, 2021.
- [8] S. Wang, Y. Teng, and P. Perdikaris, "Understanding and mitigating gradient flow pathologies in physics-informed neural networks," *SIAM Journal on Scientific Computing*, vol. 43, no. 5, pp. A3055-A3081, 2021.
- [9] R. Bischof and M. Kraus, "Multi-objective loss balancing for physics-informed deep learning," *arXiv preprint arXiv:2110.09813*, 2021.
- [10] N. Sukumar and A. Srivastava, "Exact imposition of boundary conditions with distance functions in physics-informed deep neural networks," *Computer Methods in Applied Mechanics and Engineering*, vol. 389, p. 114333, 2022.
- [11] S. Dong and N. Ni, "A method for representing periodic functions and enforcing exactly periodic boundary conditions with deep neural networks," *Journal of Computational Physics*, vol. 435, p. 110242, 2021.
- [12] S. Wang, S. Sankaran, and P. Perdikaris, "Respecting causality for training physics-informed neural networks," *Computer Methods in Applied Mechanics and Engineering*, vol. 421, p. 116813, 2024.
- [13] A. Krishnapriyan, A. Gholami, S. Zhe, R. Kirby, and M. W. Mahoney, "Characterizing possible failure modes in physics-informed neural networks," *Advances in Neural Information Processing Systems*, vol. 34, pp. 26548-26560, 2021.
- [14] J. Guo, Y. Yao, H. Wang, and T. Gu, "Pre-training strategy for solving evolution equations based on physics-informed neural networks," *Journal of Computational Physics*, vol. 489, p. 112258, 2023.
- [15] S. J. Anagnostopoulos, J. D. Toscano, N. Stergiopoulos, and G. E. Karniadakis, "Residual-based attention in physics-informed neural networks," *Computer Methods in Applied Mechanics and Engineering*, vol. 421, p. 116805, 2024.
- [16] L. D. McClenny and U. M. Braga-Neto, "Self-adaptive physics-informed neural networks," *Journal of Computational Physics*, vol. 474, p. 111722, 2023.
- [17] Y. Song, H. Wang, H. Yang, M. L. Taccari, and X. Chen, "Loss-attentional physics-informed neural networks," *Journal of Computational Physics*, vol. 501, p. 112781, 2024.
- [18] W. Li, C. Zhang, C. Wang, H. Guan, and D. Tao, "Revisiting PINNs: Generative adversarial physics-informed neural networks and point-weighting method," *arXiv preprint arXiv:2205.08754*, 2022.

- [19] A. Daw, J. Bu, S. Wang, P. Perdikaris, and A. Karpatne, "Mitigating propagation failures in physics-informed neural networks using retain-resample-release (r3) sampling," *arXiv preprint arXiv:2207.02338*, 2022.
- [20] M. A. Nabian, R. J. Gladstone, and H. Meidani, "Efficient training of physics-informed neural networks via importance sampling," *Computer -Aided Civil and Infrastructure Engineering*, vol. 36, no. 8, pp. 962-977, 2021.
- [21] F. Jiang, X. Hou, and M. Xia, "Densely Multiplied Physics Informed Neural Network," *arXiv preprint arXiv:2402.04390*, 2024.
- [22] J. Cho, S. Nam, H. Yang, S.-B. Yun, Y. Hong, and E. Park, "Separable physics-informed neural networks," *Advances in Neural Information Processing Systems*, vol. 36, 2024.
- [23] S. Wang, B. Li, Y. Chen, and P. Perdikaris, "PirateNets: Physics-informed Deep Learning with Residual Adaptive Networks," *arXiv preprint arXiv:2402.00326*, 2024.
- [24] A. Griewank and A. Walther, *Evaluating derivatives: principles and techniques of algorithmic differentiation*. SIAM, 2008.
- [25] N. Zobeiry and K. D. Humfeld, "A physics-informed machine learning approach for solving heat transfer equation in advanced manufacturing and engineering applications," *Engineering Applications of Artificial Intelligence*, vol. 101, p. 104232, 2021.
- [26] M. Tancik *et al.*, "Fourier features let networks learn high frequency functions in low dimensional domains," *Advances in neural information processing systems*, vol. 33, pp. 7537-7547, 2020.
- [27] S. Wang, S. Sankaran, H. Wang, and P. Perdikaris, "An expert's guide to training physics-informed neural networks," *arXiv preprint arXiv:2308.08468*, 2023.
- [28] X. Glorot and Y. Bengio, "Understanding the difficulty of training deep feedforward neural networks," in *Proceedings of the thirteenth international conference on artificial intelligence and statistics, 2010: JMLR Workshop and Conference Proceedings*, pp. 249-256.
- [29] G. Zhang, H. Yang, F. Zhu, and Y. Chen, "Dasa-pinns: Differentiable adversarial self-adaptive pointwise weighting scheme for physics-informed neural networks," 2023.